catalysts

Article

Development and Optimization of Air-Electrodes for Rechargeable Zn–Air Batteries

Khair Un Nisa, Williane da Silva Freitas *, Jorge Montero, Alessandra D'Epifanio and Barbara Mecheri *

Department of Chemical Sciences and Technologies, University of Rome Tor Vergata, Via della Ricerca Scientifica, 00133 Rome, Italy; nsikrn01@uniroma2.it (K.U.N.); jorge.montero@uniroma2.it (J.M.); alessandra.d.epifanio@uniroma2.it (A.D.)
* Correspondence: williane.freitas@uniroma2.it (W.d.S.F.); barbara.mecheri@uniroma2.it (B.M.)

Abstract: Rechargeable Zn–air batteries (ZABs) can play a significant role in the transition to a cleaner and more sustainable energy system due to their high theoretical energy density, high cell voltage, and environmental friendliness. ZAB's air cathode is the principal determinant in predicting the battery's overall performance, as it is responsible for catalyzing the oxygen reduction reaction (ORR) and oxygen evolution reaction (OER) during the discharging and charging process, respectively. In this work, a detailed optimization study of the architecture of the air cathode was carried out using the benchmark bifunctional oxygen electrocatalyst (Pt/C-RuO_2). The air cathode composition and architecture were optimized regarding the choice of the commercial gas diffusion layer (GDL), the effect of hot pressing the catalyst layer (CL), and the optimum pore size of the current collector. The best cathode from this study shows a maximum power density (PD_{max}) of 167 mW/cm^2, with a round trip efficiency and a voltage gap (E_{gap}) of 59.8% and 0.78 V, respectively, indicating the air cathodes preparation approach proposed in this work as a promising strategy for the improvement of the overall performance of ZABs.

Keywords: zinc–air batteries; air cathodes optimization; electrode configuration; oxygen reduction reaction; oxygen evolution reaction

check for updates

Citation: Nisa, K.U.; da Silva Freitas, W.; Montero, J.; D'Epifanio, A.; Mecheri, B. Development and Optimization of Air-Electrodes for Rechargeable Zn–Air Batteries. *Catalysts* **2023**, *13*, 1319. https://doi.org/10.3390/catal13101319

Academic Editor: Linfei Lai

Received: 5 September 2023
Revised: 19 September 2023
Accepted: 22 September 2023
Published: 23 September 2023

1. Introduction

Humankind faces several environmental issues due to the extensive use of fossil fuels, climate change being the most prominent. The dependence on fossil fuels for energy consumption should be minimized to limit further emissions of CO_2 in the atmosphere, and the fraction of electricity produced via renewables must be increased considerably [1,2], which today is limited by the absence of cheap battery technologies [3]. In this context, lithium-ion batteries are considered the most promising technology for energy storage applications and find widespread applicability in all portable electronics, electric and hybrid electric vehicles, and grid-scale energy storage systems [4,5]. Nevertheless, large-scale production of lithium-ion batteries for grid application needs to be improved for several reasons, including limited lithium availability, high cost, and poor safety [6–8]. These drawbacks motivate the search for alternative energy storage technologies, among which rechargeable metal–air batteries (MABs) emerge as a new promising class of electrical storage [9].

Although the energy-storing capabilities of Mg and Al–air batteries are comparable to Li, their low reduction potentials lead to quick self-discharge with hydrogen evolution, causing low coulombic efficiency [10,11]. Along with a more favorable reduction potential, Zn metal is abundant, economically feasible, and can be charged more efficiently in aqueous electrolytes than lithium [12]. Therefore, due to environmental and electrochemical characteristics (1218 Wh/kg energy density and 1.66 V cell voltage), Zn–air batteries (ZABs) appear to be very promising [13–17].

A rechargeable ZAB comprises a zinc anode, separator, electrolyte compartment, and an air electrode (Figure 1).

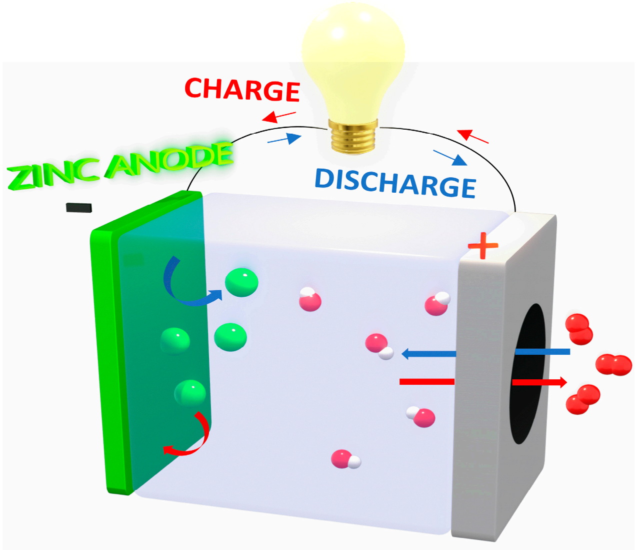

Figure 1. Schematic for a rechargeable ZAB.

During the charging and discharging process, electrochemical reactions at the zinc metal anode and the air cathode occur in an alkaline electrolyte that closes the circuit [18]. During the discharge process, the zinc anode is oxidized and converted to zincate ions $Zn(OH)_4{}^{2-}$, followed by the precipitation of ZnO, as described in Equations (1) and (2). At the air cathode, ORR occurs, with oxygen being reduced to OH^- (Equation (3)) [19]. The OER occurs at the air cathode during the charging process, and metal zinc is deposited at the anode.

Zinc electrode reaction

$$Zn + 4OH^- \rightleftharpoons Zn(OH)_4{}^{2-} + 2e^- \ (E^\circ = -1.25 \text{ V vs. SHE}) \tag{1}$$

$$Zn(OH)_4{}^{2-} \rightleftharpoons ZnO + 2OH^- + H_2O \tag{2}$$

Air electrode reaction

$$O_2 + 2H_2O + 4e^- \rightleftharpoons 4OH^- \ (E^\circ = 0.4 \text{ V vs. SHE}) \tag{3}$$

The overall reaction

$$2Zn + O_2 \rightleftharpoons 2ZnO \ (E = 1.65 \text{ V vs. SHE}) \tag{4}$$

ZAB has a standard cell potential of 1.65 V; however, its practical discharge voltage can only reach about 1.20 V. The charging voltage of the ZAB is generally higher than 2 V, which significantly reduces the energy efficiency of the ZABs [20,21]. This large charge and discharge voltage gap is mainly caused by the overpotential of the electrochemical reactions at the air electrode [22]. A bifunctional electrocatalyst must be incorporated into the air cathode [23–28] to overcome this issue. Air electrodes capable of mass and charge transport are exceedingly required to develop a rechargeable ZAB with a high round trip efficiency and power output.

Air electrodes have been extensively investigated as promising cathodes for MABs such as Li-, Mg-, Al-, and Zn–air batteries due to natural O_2 availability and the high energy density obtained from these systems. Moreover, the air electrode design offers flexibility for application in other promising electrochemical systems, such as flow reactors for CO_2 electroreduction (CO_2RR) [1,2], Li-CO_2, and Zn-CO_2 batteries [4]. One of the drawbacks of this electrode configuration is the carbonate formation from CO_2 in the air under operating conditions, which significantly affects the durability of these systems. Moreover, kinetics for the oxygen electrocatalyst are limited, and the wettability of the air cathodes is challenging to balance in aprotic solvents, making such electrodes more suitable to operate in aqueous electrolytes [18]. The primary role of an air electrode is to offer reaction sites for both ORR and OER [29]. The ORR occurs at the gas–liquid–solid triple-phase region during battery discharge. Therefore, the air electrode must have a porous structure to facilitate air diffusion and promote wettability. The balance between hydrophobicity and hydrophilicity is required to allow air to diffuse through and avoid electrolyte flooding [30]. Along with developing efficient electrocatalysts with proper wettability and durability under operating conditions, the air cathode architecture plays a decisive role in improving battery performance [31].

Air electrodes usually consist of three main parts: a catalyst layer (CL), a gas diffusion layer (GDL), and a current collector [32]. The air cathode is fabricated so that CL faces the internal liquid electrolyte compartment and GDL faces the external surroundings, while the current collector either fits in between the CL and GDL or is incorporated together with the GDL [33].

1.1. Types of Commercial Gas Diffusion Layers (GDLs) and Their Role

The role of the GDL is critical in optimizing the air electrode for ZABs. Commercial GDLs used in various electrochemical devices, such as fuel cells [34,35] and electrolyzers, typically consist of a microporous layer (MPL) adjacent to the catalyst and a macroporous layer adjacent to the air, which are both structured on a carbon-based substrate impregnated with a hydrophobic agent, usually polytetrafluoroethylene (PTFE). The PTFE-bonded carbon layers are characterized by interpenetrating microchannels of hydrophilic and hydrophobic domains, which are bounded on current collectors, usually carbon, nickel, or stainless steel mesh-based substrates [18]. They mainly differ by the presence of a thinner layer based on commercial carbon blacks such as Vulcan and carbon black pearls and PTFE, which compose the MPL [31,36]. The combination of MPL and macroporous layers in commercial GDLs offers several advantages. The MPL ensures efficient gas diffusion and water management, while the macroporous layer provides the required strength. Their porosity is also crucial since it helps mass transport through the GDL while providing a large surface area for the electrochemical reactions [18,36].

Commercial carbon cloth (CC) and carbon paper (CP) are commonly used as conductive substrates to obtain GDLs for various electrochemical devices, including ZABs [29,37,38]. CC and CP GDLs typically comprise woven porous carbon fibers that provide structural integrity to the GDL, facilitate oxygen transport from the air to the cathode reaction site, and ensure it can withstand the battery's assembly, operation, and handling processes [36,39]. Along with good electrical conductivity and enabling efficient electron transfer during electrochemical reactions [40], CC has been extensively used as an electrode substrate due to its high mechanical strength and stability. However, the choice of the carbon-based substrate depends on the specific requirements of the ZAB system, including design, performance targets, manufacturing, and cost considerations. It has been demonstrated that CP can be an efficient alternative to carbon cloth electrode substrates since it offers high surface area [41,42], modulable chemical surface, and electrochemical properties [43–45]. Moreover, the highly torturous porous structure and smooth surface of carbon papers were found to be an advantage under dry operating conditions [40], making them promise to alleviate electrolyte evaporation at the electrode side facing the air by optimizing wettability of PTFE-modified GDLs [19].

1.2. Current Collectors and Catalyst Layer (CL)

Rechargeable ZABs also require an active catalyst layer (CL) that can withstand the repeated charge and discharge cycles without significant degradation [46,47]. In most cases, the active catalyst layer covers the surface of the current collector and contacts with the electrolyte, while the gas diffusion layer lies on the reverse side and faces the surrounding air, or the current collector is placed in the middle of the active layer and gas diffusion layer and forms a sandwich structure [48].

The choice of catalyst is equally essential as it is responsible for enhancing ORR and OER during the discharging and charging of the battery. Since this study aims to optimize the air cathode architecture, benchmark ORR and OER catalysts were used. Pt supported on carbon (Pt/C) is the benchmark catalyst for ORR, exhibiting excellent ORR activity at very low loadings [34,49]. Despite its high ORR activity, durability in a highly alkaline environment (pH = 14) is compromised via Pt dissolution from the carbon support and the formation of oxide layers at high potentials, leading to a significant decrease in Pt/C activity [50–52]. In contrast, RuO_2 and IrO_2 are state-of-the-art OER catalysts due to their high activity and performance durability under hash acid and alkaline pH [53,54]. Several studies reported the combination of Pt/C and RuO_2 (Pt/C-RuO_2) for both ORR and OER at the air electrode of the rechargeable ZABs [55,56]. The amount of catalyst loaded onto the cathode substrate affects the overall performance and cost of the battery. As Pt and Ru are rare and expensive metals, decreasing the loading of such metals is desirable to combine high electrochemical activity and cost-effectiveness, promoting the large-scale commercialization of ZAB technologies [35,57–62].

In addition to the critical role of current collectors, hot-pressing the catalyst layer of the ZABs air cathodes can be an efficient approach to improve their performance and durability [63]. The hot-pressing process helps densify the CL, improve its mechanical stability, enhance gas diffusion pathways, and reduce interfacial resistance between the CL and the substrate [64]. These improvements can lead to better overall performance and durability of the ZAB's air cathode.

The role of commercial current collectors in improving the performance of ZABs must be considered, as they are crucial for efficient current distribution and electrolyte management within the battery [65]. The current collector is usually a conductive metal mesh, such as nickel foam and stainless steel [66], responsible for ensuring effective electron transfer to the external circuit, enabling the charge and discharge process in the battery [67]. SS mesh current collectors can offer several advantages over other types of current collectors in battery applications [68] due to their high electrical conductivity, corrosion resistance, large surface area for gas diffusion, and mechanical stability and structural integrity [69]. The geometry of the SS mesh, such as wire diameter and mesh pore size, can affect the overall performance of the ZABs. While defining the optimum pore size of the mesh, several factors must be considered, including electrode structure, gas diffusion requirements, and the size of ions/species involved in the electrochemical reactions. The pore size should be large enough to facilitate oxygen diffusion from the air to the cathode surface [70]. It is essential to balance the need for gas diffusion with the requirement for a high surface area and good electrode–electrolyte contact while designing an SS mesh current collector for ZABs air electrodes [71].

Since the choice of the GDL carbon-based substrates, the current collectors, and the carbon-based ink formulations for preparing both the GDL and CL are critical to boost the activity and durability of the air cathodes [48], we propose in this work a detailed optimization study related to the main components of air cathodes for zinc–air batteries, using Pt/C-RuO_2 as a benchmark bifunctional catalyst. The effect of hot pressing the catalyst layer, using carbon cloth and carbon paper for preparing the gas diffusion layers, and the different current collector mesh designs were evaluated. ZABs carrying the different cathode configurations were assembled and examined regarding their overall electrochemical performance and cycling durability.

2. Results and Discussion

Different sets of Pt/C-RuO_2-based cathodes were prepared as described in the flow diagram, along with schematics of the cathode architecture shown in Figure 2. Air-dried and hot-pressed electrodes were prepared to investigate the effect of hot-pressing the catalyst layer. Afterward, the carbon cloth used as an electrode substrate for both the catalyst layer and GDL was replaced by carbon paper, and their effect on the battery performance was investigated. Finally, the effects of a coarse (0.667 mm) and a fine (0.125 mm) pore size opening on integrating the SS mesh, as a current collector, to gas diffusion and catalyst layers were analyzed.

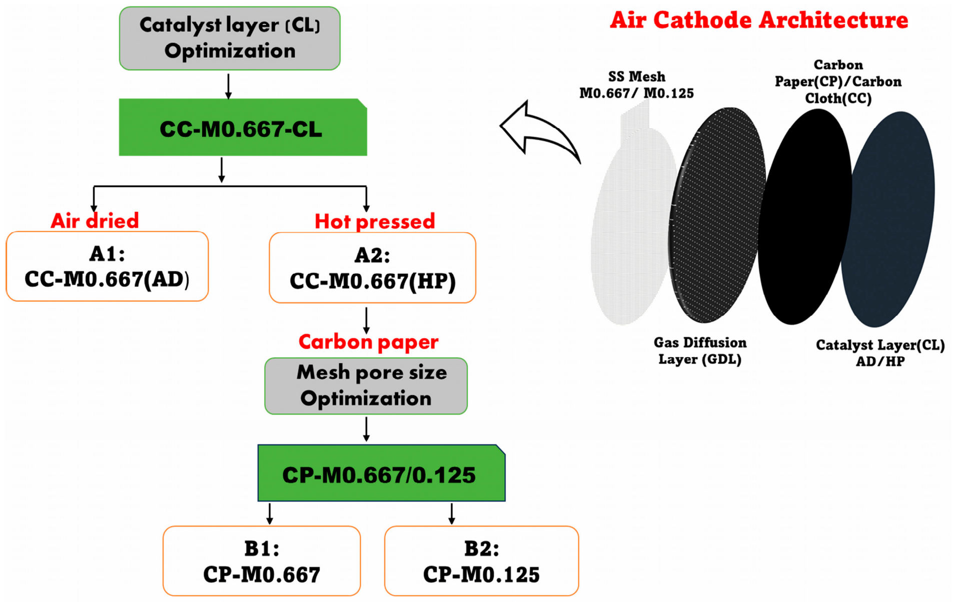

Figure 2. Air cathode architecture and a flow chart of all the prepared cathodes.

2.1. Morphology of the Prepared Gas Diffusion and Catalyst Layers

Figure 3a,b show SEM micrographs of homemade gas diffusion layers used for integrating different current collectors with commercial GDLs. As can be seen in Figure 3a, an incomplete coverage of the SS mesh current collector with a 0.667 mm pore size was observed. This feature can be related to the spilling of the GDL slurry, which can compromise the adhesion of the current collector to the commercial GDL (carbon cloth with a micro and macroporous layer), limiting mass transport through the A1, A2, and B1 cathodes. Morphology of the catalyst layer based on Pt/C and RuO_2 over the commercial MPL of the air-dried A1:CC-M0.667 (AD) and the hot-pressed A2:CC-M0.667 (HP) cathodes is characterized by a porous structure composed by the RuO_2 and carbon support particles ranging between 50 and 100 μm, with the smaller Pt particles (bright dots) distributed over the carbon support (Figure S1a,b), in good agreement with the literature [72]. Despite the similar morphology at high magnification (200 kX), the micrographs at low magnification (800 X) indicated that the catalyst layer hot-pressing step resulted in a smoother surface of the catalysts layer over the carbon cloth MPL (Figure 3c,d). Replacement of the carbon cloth by a carbon paper electrode substrate preserved the catalyst layer morphology, as indicated by comparing the micrographs in Figure 3d,e and Figure S1b,c.

Moreover, using an SS mesh with a smaller pore size (0.125 mm) enhanced the SS/GDL interface (Figure 3b) as compared to using the largest pore size (0.667 mm) SS (Figure 3a). This change also led to a smoother catalyst layer surface of the B2:CP-M0.125 cathode (Figure 3f). Using a smaller SS pore size effectively prevented the GDL from spilling from the SS mesh, ensuring a uniform coverage of the current collector. Noteworthy, the combination of the SS mesh with the smaller pore size (0.125 vs. 0.667 mm) and thickness (325 vs. 554 μm) together with the carbon paper significantly reduced the overall electrode thickness, as indicated by the micrographs of the cross-section zones of B1:CP-M0.667 and B2:CP-M0.125, showed in Figure S1e,f. B1:CP-M0.667 had a thickness of around 860 μm, while B2:CP-M0.125 was approximately 550 μm. Cross-section micrographs shown as insets in Figure 3e,f for B1:CP-M0.667 and B2:CP-M0.125, respectively, also indicate that the lower thickness and different design of the wires for the SS mesh 0.125 mm pore size, improved the adhesion of the homemade gas diffusion layer to the SS mesh. SEM analysis revealed the effective combination of the catalyst layer hot-pressing step and carbon paper, as commercial GDL, and the SS mesh 0.125 mm pore size. This combination successfully achieved air cathodes with adequate coverage, adhesion of the GDL materials to the current collector, and a smoother catalyst layer surface. These features are required to decrease the electrode resistance and improve the air cathodes' mass transport, active surface area, and durability [19].

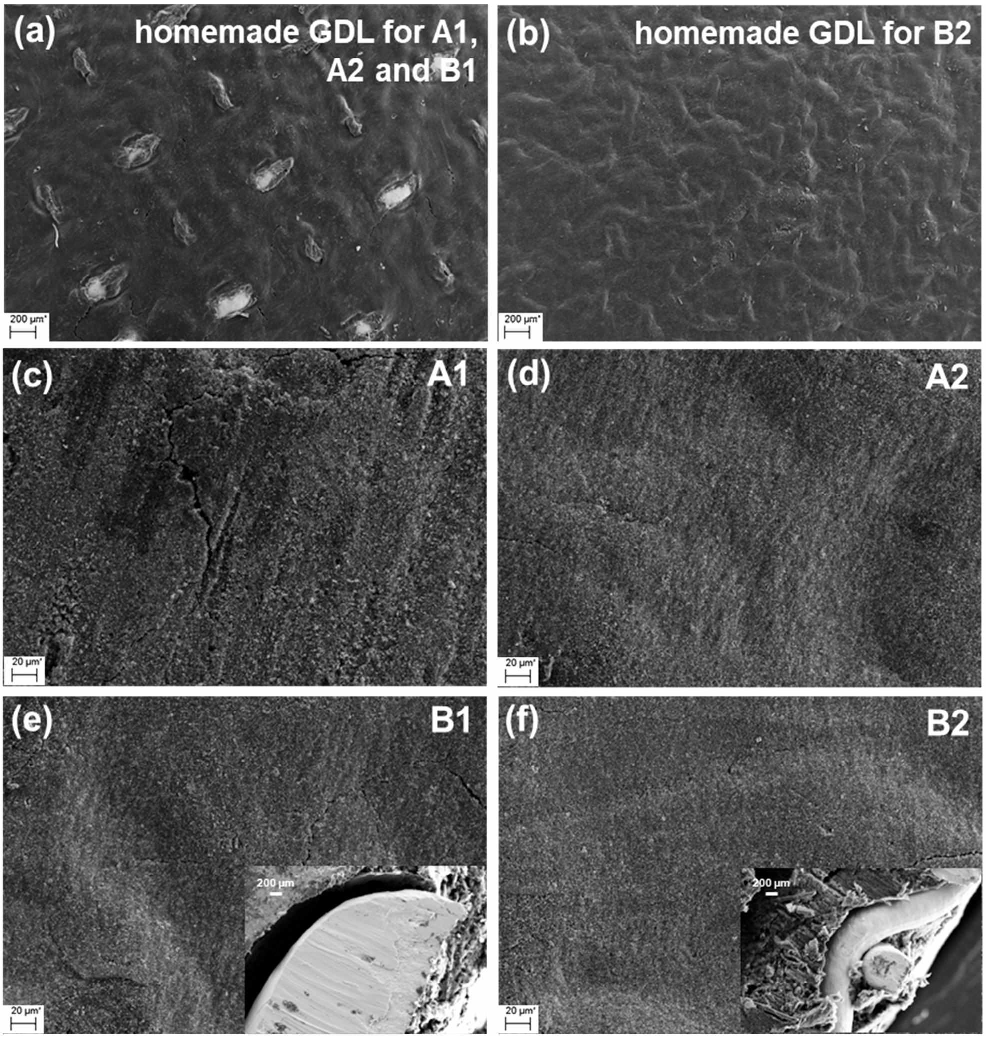

Figure 3. SEM micrographs at an 80 X magnification for the homemade GDL deposited on a SS mesh with (**a**) 0.667 mm and (**b**) 0.125 mm pore size. Catalyst layer surface of (**c**) A1, (**d**) A2, (**e**) B1, and B2 (**f**) cathodes at an 800 X magnification, with the correspondent cross sections micrographs for B1 and B2 (inset of Figure 3e,f) focused on the homemade GDL and the SS mesh.

2.2. Catalyst Layer Optimization

Two series of air cathodes, A1:CC-M0.667 (AD) and A2:CC-M0.667 (HP), were prepared utilizing carbon cloth as an electrode substrate and SS mesh with a 0.667 mm pore size as a current collector to investigate the effect of hot-pressing the catalyst layer on activity and durability of the air cathodes during operating conditions of the ZABs. Power density and polarization curves, together with the percentage increment of the maximum power density and round trip efficiency for A1:CC-M0.667 (AD) and A2:CC-M0.667 (HP) cathodes, are shown in Figure 4. The A2:CC-M0.667 (HP) cathode showed higher performance in terms of PD_{max} (121 vs. 105 mW/cm^2) (Figure 4a), with a 13 % increment (Figure 4b) as compared to A1:CC-M0.667 (AD). Moreover, the cyclability test for A1:CC-M0.667 (AD) showed a significant increase in E_{gap} after 12 h of operation, reaching a value of 1.47 V by the end of the experiment (Figure 4c). On the other hand, A2:CC-M0.667 remained remarkably stable throughout the charge–discharge cycling experiment, achieving an E_{gap} of 0.83 V after 24 h. Round trip efficiency after 24 h (Figure 4d) was also higher for the A2:CC-M0.667 as compared to the A1:CC-M0.667 (AD) cathode (57.9% vs. 39.1%), indicating a higher charging power storage for the hot-pressed cathode. The improved energy output and durability over the charge and discharge cycles achieved for the A2:CC-M0.667 are in good agreement with the SEM analysis that showed a smoother catalyst layer on the carbon cloth microporous layer after being hot pressed. These results can also be related to a higher adhesion between the CL and the carbon cloth used as an electrode substrate, reducing the CL thickness and the interfacial resistance while improving the mechanical stability, gas diffusion pathways, and electron transfer between the catalyst and the GDL [73].

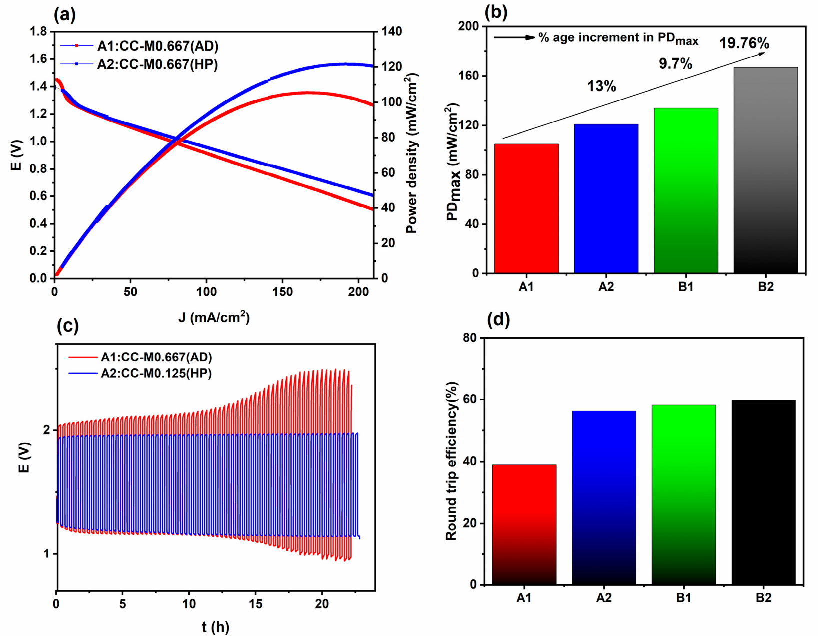

Figure 4. (**a**) Power density and polarization curves and (**b**) charge and discharge voltage cycles for A1 and A2 cathodes, (**c**) PD_{max} increment percentage, and (**d**) round trip efficiency for A1, A2, B1, and B2 cathodes.

2.3. Commercial GDL and SS Mesh Pore Size Optimization

The best-performing A2:CC-M0.667 (HP) cathode was modified by replacing carbon cloth with carbon paper and labeled as B1:CP-M0.667. As shown in Figure 5a, the PDmax was higher (134 mW/cm^2) for the B1:CP-M0.667 cathode, with an increment of 9.7% compared to A2:CC-M0.667 (HP). The E_{gap} was also reduced from 0.83 V to 0.81 V after 24 h, as shown in Figure 5b, with a slight increase in the round trip efficiency (58.2% vs. 57.9%) for B1:CP-M0.667, indicating that carbon paper was a more effective electrode substrate than carbon cloth. The performance improvement can be ascribed to the lower thickness and higher porosity of carbon paper compared to carbon cloth, which promotes oxygen transport through the GDL to the catalyst layer, affecting the overall efficiency of oxygen utilization within the battery and potentially increasing its power density. Furthermore, the optimized wettability of the carbon paper, under the ZABs operating conditions, can contribute to minimizing electrolyte flooding and evaporation loss at the electrode side facing the air, improving the battery performance [19]. To promote a higher adhesion and a more homogeneous distribution of the GDL and CL onto the current collector and a consequent decrease of the cell resistance and performance improvement, an SS mesh with a smaller pore size (0.125 mm) was also evaluated as an alternative to the mesh with a 0.667 mm pore size. Polarization and power density curves (Figure 5a) for the B2:CP-M0.125 cathode indicated that maximum power density increased by 19.76% with a smaller SS mesh pore size, reaching 167 mW/cm^2. Cyclability of B2:CP-M0.125 was also improved, as pointed out by a lower E_{gap} (0.78 V), as shown in Figure 5b,c, with a round trip efficiency of 59.8% after 24 h. The morphology of the catalyst surface of the B2:CP-M0.125 cathode slightly changed after charge and discharge cycling, with the presence of small cavities non-homogeneously distributed at the surface, promoting agglomeration of the catalyst particles. This is in good agreement with other studies that showed a typical degradation of the catalyst layer, primarily due to corrosion of the carbon support, after aging in highly alkaline solutions [74]. The observed performance improvement is associated with the adequate coverage of the current collector adhesion of the GDLs, which affects the catalyst immobilization, mechanical and electrochemical durability, and diffusion of the electroactive species [64].

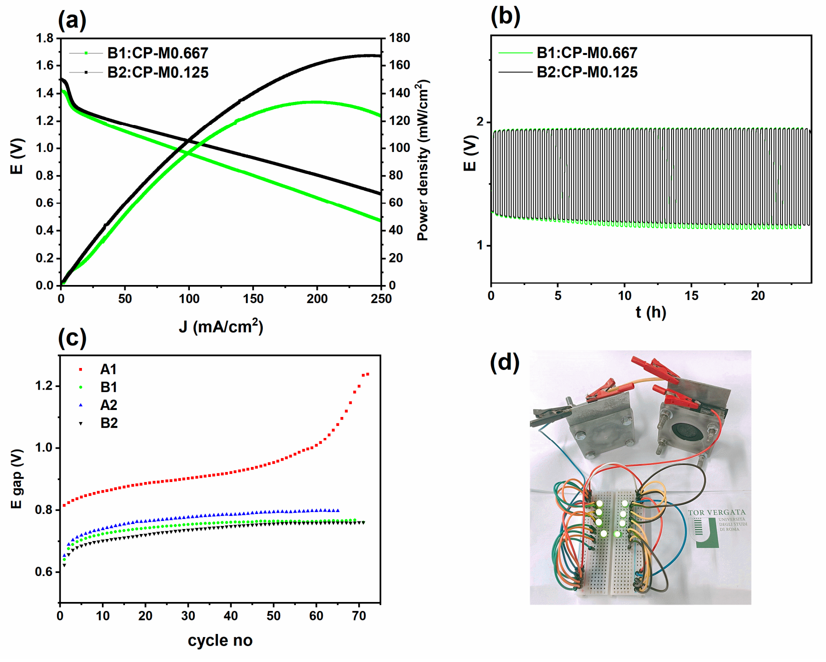

Figure 5. (**a**) Power density and polarization curves and (**b**) charge and discharge voltage cycles for B1 and B2 cathodes, (**c**) E_{gap} (V) for A1, A2, B1, and B2 cathodes vs. cycle number (n), (**d**) photograph of several LED lights powered by two assembled ZABs utilizing B2 cathode.

Figure 5d shows a picture of several LED lights powered by two assembled ZABs utilizing the optimized B2:CP-M0.125 cathode. Table 1 summarizes the electrochemical performance of the ZABs assembled with the air cathodes prepared in this work. Table 2 compares performance with ZABs reported in the literature assembled with benchmark Pt/C-RuO_2 air cathodes. This comparison highlights our approach as an efficient alternative to boost the performance of ZABs.

Table 1. Performance comparison of A1, A2, B1, and B2 cathodes of ZAB's tests.

Pt/C-RuO_2-Based Air Cathodes		**PD_{max} (mW/cm^2)**	**Charge Potential(V)**	**Discharge Potential (V)**	**E_{gap} (V)**	**Round Trip Efficiency (%)**
A1	CC-M0.667(AD)	105 ± 0.2	2.43	0.95	1.47 ± 0.2	39.1
A2	CC-M0.125(HP)	121 ± 1.0	1.97	1.14	0.83 ± 0.3	57.9
B1	CP-M0.667	134 ± 1.2	1.94	1.13	0.81 ± 0.1	58.2
B2	CP-M0.125	167 ± 0.3	1.94	1.16	0.78 ± 0.05	59.8

Table 2. Performance comparison of the Pt/C-RuO_2-based cathodes for rechargeable ZABs from the existing literature.

Pt/C-RuO_2-Based Cathodes(V)	E_{gap}	Durability Hours/No. of Cycles (n) @J(mA/cm^2)	PD_{max} (mW/cm^2)	References
1	1.45	28h@10	110	[56]
2	1.30	110h@5	112	[75]
3	1.70	35h@10	75	[76]
4	1.10	20h@5	129	[77]
5	1.69	300cycles@10	82	[78]
6	1.16	72cycles@4	-	[79]
7	1.60	24h@10	40	[80]
8	0.78	24h/75cycles@5	167	This work

3. Materials and Methods

3.1. Materials

Zinc foil (Goodfellow), zinc acetate (99%), potassium hydroxide (KOH, 85%), Pt/C (20 wt.% Pt), RuO_2, Nafion (5 wt.%) solution, and polytetrafluoroethylene (PTFE, 60 wt.% dispersion in H_2O) were purchased from Sigma–Aldrich (St. Louis, MO, United States). Carbon Vulcan XC 72R was supplied by the CABOT Corporation (Boston, MA, USA), 304 stainless steel mesh #30 (0.667 mm pore Size) and 304 stainless steel woven wire #120 mesh (0.125 mm pore size) were used as current collectors. Carbon paper 38-BC (thickness = 325 µm, porosity percentage = 80%) and carbon cloth ELAT 1400 (thickness = 554 µm, porosity percentage = 65%) were supplied by SGL TECHNOLOGIES GmbH (Bonn, Germany) and Quintech (Göppingen, Germany), respectively, and were used as gas diffusion layer substrate.

3.2. Preparation of Air Cathodes for Rechargeable ZABs

3.2.1. Preparation of the Homemade Gas Diffusion Layer

Stainless steel (SS) meshes were used as current collectors and modified with a gas diffusion layer (GDL) as follows: 300 mg of carbon Vulcan were dispersed in 4 mL of ethanol containing 400 µL of PTFE emulsion (40 wt.% dispersion in H_2O). The obtained thick paste was homogenously spread with the help of a spatula on SS mesh (7 cm^2) and dried in an oven at 40 °C for 5 min. The SS mesh containing GDL was hot pressed twice (80 °C and 4.96 MPa) for 1 min. Then, CP/CC was placed on the GDL-modified SS mesh and hot pressed (under 80 °C and 4.96 MPa) for 1 min.

3.2.2. Preparation of the Catalyst Layer

The catalyst layer was prepared by dispersing 24 mg of a catalyst into a Nafion 5 wt.% (160 µL) and isopropanol solution (200 µL). The ink was deposited to the CC or CP surface through four successive brush-painted layers, allowing each to fully dry before the next was applied to a catalyst loading of 2 mg/cm^2. The Nafion content was 33 wt.% relative to the solid weights of the catalysts. The prepared cathodes were subjected to two different treatments: air-drying overnight (A1:CC-M0.667 (AD)) or hot pressing at 80 °C under a pressure of 4.96 MPa for 2 min, for cathodes A2:CC-M0.667 (HP), B1:CP-M0.667, and B2:CP-M0.125.

3.3. Methods

ZAB tests were performed by assembling the air cathodes prepared as described in Section 3.2 into an in-house ZAB prototype, realized by sealing four plexiglass (5 × 5 × 0.5 cm) sheets with Viton rubber gaskets, as shown in Figure 6. A 1 mm thick zinc foil served as an anode, and 7 mL of an aqueous solution of 0.2 M Zn $(CH_3COO)_2$ in 6.0 M KOH was used as an electrolyte. The performance of the ZABs was evaluated regarding polarization and power density curves acquired via steady-state galvanostatic polarization experiments. The entire battery test was performed at room temperature. Polarization and power density curves were obtained using a multichannel VSP potentiostat/galvanostat (BioLogic, Seyssinet-Pariset, France) connected to a personal computer operating the EC-Lab software. The tests were carried out using a two-electrode configuration with the cathode connected to the working electrode channel and the anode connected to the counter and reference electrode channel. The cycling stability and efficiency were evaluated via the galvanostatic charge–discharge mode at a current density of 5 mA/cm^2 for 20 min per cycle. The polarization curves were recorded through a linear sweep voltammetry (LSV) test using a scan rate of 100 mV/s. The power density and current density generated by ZABs were normalized to the cathode geometric surface area of 3.14 cm^2.

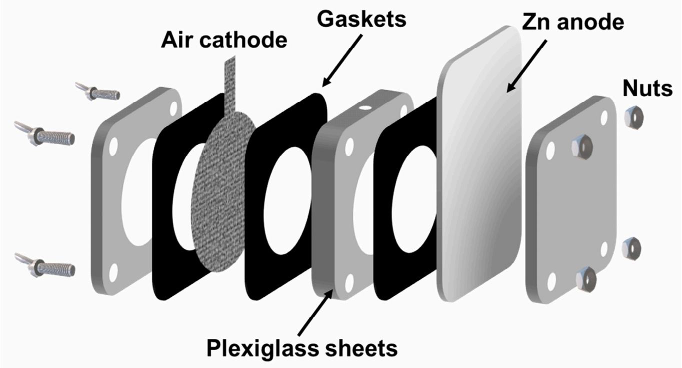

Figure 6. Schematic for the assembly of an in-house rechargeable ZAB.

The electrochemical parameters used to evaluate the performance of the ZABs include voltage gap (E_{gap}), round trip efficiency, durability, and power density. The round trip efficiency is the energy-utilizing efficiency of the ZABs and is estimated by dividing the voltage of the discharge process by the voltage of the charging process. E_{gap} is measured by measuring the difference between charging and discharging curves obtained during a galvanostatic measurement.

The morphology of the homemade GDLs and prepared air cathodes was investigated using a scanning electron microscope (FE-SEM, Leo Supra 35, Carl Zeiss, Oberkochen, Germany).

4. Conclusions

Different air-cathode families were prepared using Pt/C-RuO_2 as a bifunctional catalyst towards ORR and OER. A detailed optimization study of the air-cathode architecture was carried out to improve the overall performance of ZABs. This study showed that the catalyst layer hot-pressing step enhanced the performance of the assembled ZABs, particularly in terms of durability over the charge and discharge cycles. It can be ascribed as the effect of a smoother distribution of the Pt/C-RuO_2 catalysts over the carbon cloth microporous layer. Moreover, using carbon paper alternatively to carbon cloth as electrode substrate preserved the catalyst layer morphology and improved battery performance. It can be related to the carbon paper's lower thickness and higher porosity, positively affecting oxygen transport and electron transfer at the cathode. Utilizing an SS mesh with a 0.125 mm pore size potentially increased the power density of the ZABs. The smaller pore size prevented the escaping of the GDL slurry through the SS mesh, leading to its adequate coverage and adhesion of the materials composing the GDLs to the current collector. These features impact gas diffusion, effective electrolyte distribution, and catalyst immobilization. The optimized B2:CP-M0.125 cathode reached a high maximum power density (167 mW/cm^2) and a small E_{gap} (0.78 V) after 24 h of cycling, indicating the high performance achieved with the optimized electrode architecture, in comparison to the literature studies dealing with Pt/C-RuO_2-based air cathodes. The optimized architecture of bifunctional platinum–group–metal (PGM)-based air cathodes can be utilized for other PGM-free bifunctional oxygen electrocatalysts in rechargeable ZABs.

Supplementary Materials: The following supporting information can be downloaded at: https://www.mdpi.com/article/10.3390/catal13101319/s1, Figure S1: SEM micrographs for the catalyst layer surface of A1, A2, B1, and B2, together with the cross-section micrographs for B1 and B2 cathodes, are provided as supplementary material. Figure S2: SEM micrographs for the catalyst layer surface of the B2 cathode after charge and discharge cycling.

Author Contributions: Conceptualization, W.d.S.F., A.D. and B.M.; data curation, K.U.N., W.d.S.F. and B.M.; funding acquisition, A.D.; investigation, K.U.N., J.M. and W.d.S.F.; methodology, K.U.N., W.d.S.F. and B.M.; project administration, B.M.; resources, A.D. and B.M.; supervision, W.d.S.F., A.D. and B.M.; writing—original draft, K.U.N., J.M. and W.d.S.F.; Writing—review and editing, W.d.S.F. and B.M. All authors have read and agreed to the published version of the manuscript.

Funding: This work was supported in part by the Italian Ministry of Foreign Affairs and International Cooperation, grant number CN23GR06.

Data Availability Statement: Data used to support the findings of this study are available within the article and its Supplementary Materials.

Conflicts of Interest: The authors declare no conflict of interest.

References

1. Koolen, C.D.; Luo, W.; Züttel, A. From Single Crystal to Single Atom Catalysts: Structural Factors Influencing the Performance of Metal Catalysts for CO_2 Electroreduction. *ACS Catal.* **2023**, *13*, 948–973. [CrossRef]
2. Xie, J.; Wang, Y. Recent Development of CO_2 Electrochemistry from Li-CO_2 Batteries to Zn-CO_2 Batteries. *Acc. Chem. Res.* **2019**, *52*, 1721–1729. [CrossRef]
3. Montero, J.; Navalpotro, P.; D'Epifanio, A.; Mecheri, B.; Licoccia, S.; Carretero-González, J. Redox-Active Coordination Polymers as Bifunctional Electrolytes in Slurry-Based Aqueous Batteries at Neutral pH. *J. Electroanal. Chem.* **2021**, *895*, 115442. [CrossRef]
4. Zhang, J.; Pham, T.H.M.; Ko, Y.; Li, M.; Yang, s.; Koolen, C.D.; Zhong, L.; Luo, W.; Züttel, A. Tandem effect of Ag@C@Cu catalysts enhances ethanol selectivity for electrochemical CO_2 reduction in flow reactors. *Cell Rep. Phys. Sci.* **2022**, *3*, 100949. [CrossRef]
5. Montero, J.; da Silva Freitas, W.; Mecheri, B.; Forchetta, M.; Galloni, P.; Licoccia, S.; D'Epifanio, A. A Neutral-pH Aqueous Redox Flow Battery Based on Sustainable Organic Electrolytes. *ChemElectroChem* **2023**, *10*, e202201002. [CrossRef]
6. He, J.; Meng, J.; Huang, Y. Challenges and Recent Progress in Fast-Charging Lithium-Ion Battery Materials. *J. Power Sources* **2023**, *570*, 232965. [CrossRef]
7. Wang, Q.-C.; Meng, J.-K.; Yue, X.-Y.; Qiu, Q.-Q.; Song, Y.; Wu, X.-J.; Fu, Z.-W.; Xia, Y.-Y.; Shadike, Z.; Wu, J.; et al. Tuning P2-Structured Cathode Material by Na-Site Mg Substitution for Na-Ion Batteries. *J. Am. Chem. Soc.* **2019**, *141*, 840–848. [CrossRef]
8. Zhang, M.-H.; Meng, J.-K.; Xiao, N.; Shao, R.-W.; Wu, X.-J.; Gao, P.; Shadike, Z.; Zhou, Y.-N. Sodium Storage Mechanism of a GeP5/C Composite as a High Capacity Anode Material for Sodium-Ion Batteries. *Chem. Commun.* **2022**, *58*, 10345–10348. [CrossRef]
9. Yue, X.-Y.; Wang, W.-W.; Wang, Q.-C.; Meng, J.-K.; Wang, X.-X.; Song, Y.; Fu, Z.-W.; Wu, X.-J.; Zhou, Y.-N. Cuprite-Coated Cu Foam Skeleton Host Enabling Lateral Growth of Lithium Dendrites for Advanced Li Metal Batteries. *Energy Stor. Mater.* **2019**, *21*, 180–189. [CrossRef]
10. Yang, Y.; Zhou, J.; Wang, L.; Jiao, Z.; Xiao, M.; Huang, Q.; Liu, M.; Shao, Q.; Sun, X.; Zhang, J. Prussian Blue and Its Analogues as Cathode Materials for Na-, K-, Mg-, Ca-, Zn- and Al-Ion Batteries. *Nano Energy* **2022**, *99*, 107424. [CrossRef]
11. Wang, H.-F.; Xu, Q. Materials Design for Rechargeable Metal-Air Batteries. *Matter* **2019**, *1*, 565–595. [CrossRef]
12. Lee, J.; Kim, S.; Cao, R.; Choi, N.-S.; Liu, M.; Lee, K.T.; Cho, J. Metal-Air Batteries with High Energy Density: Li-Air versus Zn–air. *Adv. Energy Mater.* **2011**, *1*, 34–50. [CrossRef]
13. Han, Y.; Zhou, C.; Wang, B.; Li, Y.; Zhang, L.; Zhang, W.; Huang, Y.; Zhang, R. Rational Design of Advanced Oxygen Electrocatalysts for High-Performance Zinc-Air Batteries. *Chem Catal.* **2022**, *2*, 3357–3394. [CrossRef]
14. Radenahmad, N.; Khezri, R.; Mohamad, A.A.; Nguyen, M.T.; Yonezawa, T.; Somwangthanaroj, A.; Kheawhom, S. A Durable Rechargeable Zinc-Air Battery via Self-Supported MnOx-S Air Electrode. *J. Alloys Compd.* **2021**, *883*, 160935. [CrossRef]
15. Abbasi, A.; Xu, Y.; Abouzari-Lotf, E.; Etesami, M.; Khezri, R.; Risse, S.; Kardjilov, N.; Van Tran, K.; Jia, H.; Somwangthanaroj, A.; et al. Phosphonated Graphene Oxide-Modified Polyacrylamide Hydrogel Electrolytes for Solid-State Zinc-Ion Batteries. *Electrochim. Acta* **2022**, *435*, 141365. [CrossRef]
16. Khezri, R.; Motlagh, S.R.; Etesami, M.; Mohamad, A.A.; Pornprasertsuk, R.; Olaru, S.; Kheawhom, S. High Current Density Charging of Zinc-Air Flow Batteries: Investigating the Impact of Flow Rate and Current Density on Zinc Electrodeposition. *Appl. Energy* **2023**, *348*, 121564. [CrossRef]
17. Bósquez-Cáceres, M.F.; De Lima, L.; Morera Córdova, V.; Delgado, A.D.; Béjar, J.; Arjona, N.; Álvarez-Contreras, L.; Tafur, J.P. Chitosan-Carboxymethylcellulose Hydrogels as Electrolytes for Zinc-Air Batteries: An Approach to the Transition towards Renewable Energy Storage Devices. *Batteries* **2022**, *8*, 265. [CrossRef]
18. Li, Y.; Dai, H. Recent Advances in Zinc-Air Batteries. *Chem. Soc. Rev.* **2014**, *43*, 5257–5275. [CrossRef]

19. Pan, J.; Xu, Y.Y.; Yang, H.; Dong, Z.; Liu, H.; Xia, B.Y. Advanced Architectures and Relatives of Air Electrodes in Zn–air Batteries. *Adv. Sci.* **2018**, *5*, 1700691. [CrossRef]
20. Yao, Z.C.; Tang, T.; Hu, J.S.; Wan, L.J. Recent Advances on Nonprecious-Metal-Based Bifunctional Oxygen Electrocatalysts for Zinc-Air Batteries. *Energy Fuels* **2021**, *35*, 6380–6401. [CrossRef]
21. Dong, F.; Wu, M.; Chen, Z.; Liu, X.; Zhang, G.; Qiao, J.; Sun, S. Atomically Dispersed Transition Metal-Nitrogen-Carbon Bifunctional Oxygen Electrocatalysts for Zinc-Air Batteries: Recent Advances and Future Perspectives. *Nano-Micro Lett.* **2022**, *14*, 36. [CrossRef]
22. Li, W.; Cheng, L.; Chen, X.; Liu, Y.; Liu, Y.; Liu, Q.; Huang, Y. Key Materials and Structural Design in Flexible and Stretchable Zinc-Air Batteries. *Nano Energy* **2023**, *106*, 108039. [CrossRef]
23. Béjar, J.; Delgado, A.D.; Espinosa-Magaña, F.; Aguilar-Elguezabal, A.; Guerra-Balcázar, M.; Arjona, N.; Álvarez-Contreras, L. Electrodeposition of Smallsized NiM2O4 Spinels (M: Co, Mn) as Bifunctional Nanomaterials for Rechargeable Zinc-Air Batteries. *J. Alloys Compd.* **2022**, *929*, 167266. [CrossRef]
24. Zhang, L.; Pang, D.; Cao, X.; Ma, Y.; Kou, Y.; Liu, Z.; Hassan, A.; Guo, C.; Yue, F.; Wang, J. Phosphorus Modified Hollow, Porous Nickel-Cobalt Oxides Nanocubes with Heterostructure for Oxygen Evolution Reaction in Alkaline. *J. Alloys Compd.* **2022**, *925*, 166338. [CrossRef]
25. Li, S.; Xie, Y.; Feng, C.; Hassan, A.; Wang, J. Nitrogen-Rich Porous Carbon Nanotubes Coated Co/Mo_2N Composites Derived from Metal-Organic Framework as Efficient Bifunctional Oxygen Electrocatalysts. *Catalysts* **2023**, *13*, 801. [CrossRef]
26. Xie, Y.; Feng, C.; Guo, Y.; Hassan, A.; Li, S.; Zhang, Y.; Wang, J. Dimethylimidazole and Dicyandiamide Assisted Synthesized Rich-Defect and Highly Dispersed CuCo-Nx Anchored Hollow Graphite Carbon Nanocages as Efficient Trifunctional Electrocatalyst in the Same Electrolyte. *J. Power Sources* **2022**, *517*, 230721. [CrossRef]
27. Qiao, S.; Guo, J.; Wang, D.; Zhang, L.; Hassan, A.; Chen, T.; Feng, C.; Zhang, Y.; Wang, J. Core-Shell Cobalt Particles Co@CoO Loaded on Nitrogen-Doped Graphene for Photocatalytic Water-Splitting. *Int. J. Hydrog. Energy* **2020**, *45*, 1629–1639. [CrossRef]
28. Béjar, J.; Espinosa-Magaña, F.; Avelar, J.; Aguilar-Elguezabal, A.; Guerra-Balcázar, M.; Arjona, N.; Álvarez-Contreras, L. Rational Design of Nitrogen-doped Carbon Nanotubes by Defect Engineering for Zn–air Batteries with High Performance. *Carbon* **2023**, *204*, 411–426. [CrossRef]
29. Davari, E.; Ivey, D. Bifunctional Electrocatalysts for Zn–air Batteries. *Sustain. Energy Fuels* **2017**, *2*, 39–67. [CrossRef]
30. da Silva Freitas, W.; Gemma, D.; Mecheri, B.; D'Epifanio, A. Air-Breathing Cathodes for Microbial Fuel Cells Based on Iron-Nitrogen-Carbon Electrocatalysts. *Bioelectrochemistry* **2022**, *146*, 108103. [CrossRef]
31. Sumboja, A.; Lübke, M.; Wang, Y.; An, T.; Zong, Y.; Liu, Z. All-Solid-State, Foldable, and Rechargeable Zn–air Batteries Based on Manganese Oxide Grown on Graphene-Coated Carbon Cloth Air Cathode. *Adv. Energy Mater.* **2017**, *7*, 1700927. [CrossRef]
32. Wang, P.; Wan, L.; Lin, Y.; Wang, B. Construction of Mass-Transfer Channel in Air Electrode with Bifunctional Catalyst for Rechargeable Zinc-Air Battery. *Electrochim. Acta* **2019**, *320*, 134564. [CrossRef]
33. Cai, X.; Lai, L.; Lin, J.; Shen, Z. Recent Advances in Air Electrodes for Zn–air Batteries: Electrocatalysis and Structural Design. *Mater. Horiz.* **2017**, *4*, 945–976. [CrossRef]
34. da Silva Freitas, W.; D'Epifanio, A.; Lo Vecchio, C.; Gatto, I.; Baglio, V.; Ficca, V.C.A.; Placidi, E.; Mecheri, B. Tailoring MOF Structure via Iron Decoration to Enhance ORR in Alkaline Polymer Electrolyte Membrane Fuel Cells. *J. Chem. Eng.* **2023**, *465*, 142987. [CrossRef]
35. Ricciardi, B.; Mecheri, B.; da Silva Freitas, W.; Ficca, V.C.A.; Placidi, E.; Gatto, I.; Carbone, A.; Capasso, A.; D'Epifanio, A. Porous Iron-Nitrogen-Carbon Electrocatalysts for Anion Exchange Membrane Fuel Cells (AEMFC). *ChemElectroChem* **2023**, *10*, e202201115. [CrossRef]
36. Park, S.; Park, Y. Fabrication of Gas Diffusion Layer (GDL) Containing Microporous Layer Using Flourinated Ethylene Prophylene (FEP) for Proton Exchange Membrane Fuel Cell (PEMFC). *Int. J. Precis. Eng. Manuf.* **2012**, *13*, 1145–1151. [CrossRef]
37. Sumboja, A.; Ge, X.; Goh, F.W.T.; Li, B.; Geng, D.; Hor, T.S.A.; Zong, Y.; Liu, Z. Manganese Oxide Catalyst Grown on Carbon Paper as an Air Cathode for High-Performance Rechargeable Zinc-Air Batteries. *ChemPlusChem* **2015**, *80*, 1341–1346. [CrossRef]
38. Meng, J.-K.; Wang, W.-W.; Yue, X.-Y.; Xia, H.-Y.; Wang, Q.-C.; Wang, X.-X.; Fu, Z.-W.; Wu, X.-J.; Zhou, Y.-N. Cotton-Derived Carbon Cloth Enabling Dendrite-Free Li Deposition for Lithium Metal Batteries. *J. Power Sources* **2020**, *465*, 228291. [CrossRef]
39. Zhang, S.; Xiao, S.; Li, D.; Liao, J.; Ji, F.; Liu, H.; Ci, L. Commercial Carbon Cloth: An Emerging Substrate for Practical Lithium Metal Batteries. *Energy Storage Mater.* **2022**, *48*, 172–190. [CrossRef]
40. Wang, Y.; Wang, C.-Y.; Chen, K. Elucidating Differences between Carbon Paper and Carbon Cloth in Polymer Electrolyte Fuel Cells. *Electrochim. Acta* **2007**, *52*, 3965–3975. [CrossRef]
41. Li, M.; Xiong, D.; Liu, W.; Liu, J.; Dai, L.; Xiao, X. Boronised Electrodeposited Nickel on Carbon Paper for the Oxygen Evolution Reactions. *Mater. Lett.* **2023**, *336*, 133867. [CrossRef]
42. Shi, Q.; Feng, C.; Tang, F.; Li, B.; Ming, P.; Zhang, C. Bulk Resistance and Internal Contacts of Carbon Fiber Paper Determined via X-Ray Computed Tomography. *Mater. Chem. Phys.* **2023**, *296*, 127137. [CrossRef]
43. Ji, H.; Wang, M.; Liu, S.; Sun, H.; Liu, J.; Qian, T.; Yan, C. Pyridinic and Graphitic Nitrogen-Enriched Carbon Paper as a Highly Active Bifunctional Catalyst for Zn–air Batteries. *Electrochim. Acta* **2020**, *334*, 135562. [CrossRef]
44. Ma, T.Y.; Ran, J.; Dai, S.; Jaroniec, M.; Qiao, S.Z. Phosphorus-Doped Graphitic Carbon Nitrides Grown In Situ on Carbon-Fiber Paper: Flexible and Reversible Oxygen Electrodes. *Angew. Chem. Int. Ed.* **2015**, *54*, 4646–4650. [CrossRef]

45. Levinas, R.; Tsyntsaru, N.; Cesiulis, H. Insights into Electrodeposition and Catalytic Activity of MoS2 for Hydrogen Evolution Reaction Electrocatalysis. *Electrochim. Acta* **2019**, *317*, 427–436. [CrossRef]
46. Kong, S.; Xiang, X.; Jin, B.; Guo, X.; Wang, H.; Zhang, G.; Huang, H.; Cheng, K. B, O and N Codoped Biomass-Derived Hierarchical Porous Carbon for High-Performance Electrochemical Energy Storage. *Nanomaterials* **2022**, *12*, 1720. [CrossRef]
47. Zhang, G.; Zhang, P.; Kong, S.; Jin, B. Spinel LiMn2O4 as Electrocatalyst toward Solid-State Zinc-Air Batteries. *Catalysts* **2023**, *13*, 860. [CrossRef]
48. Tomboc, G.M.; Yu, P.; Kwon, T.; Lee, K.; Li, J. Ideal Design of Air Electrode-A Step Closer toward Robust Rechargeable Zn–air Battery. *APL Mater.* **2020**, *8*, 050905. [CrossRef]
49. Jaouen, F.; Jones, D.; Coutard, N.; Artero, V.; Strasser, P.; Kucernak, A. Toward Platinum Group Metal-Free Catalysts for Hydrogen/Air Proton-Exchange Membrane Fuel Cells. *Johns. Matthey Technol. Rev.* **2018**, *62*, 231–255. [CrossRef]
50. Wu, Z.; Gao, Y.; Wang, Z.; Xiao, W.; Wang, X.; Li, B.; Li, Z.; Liu, X.; Ma, T.; Wang, L. Surface-Enriched Ultrafine Pt Nanoparticles Coupled with Defective CoP as Efficient Trifunctional Electrocatalyst for Overall Water Splitting and Flexible Zn–air Battery. *Chin. J. Catal.* **2023**, *46*, 36–47. [CrossRef]
51. da Silva Freitas, W.; D'Epifanio, A.; Ficca, V.C.A.; Placidi, E.; Arciprete, F.; Mecheri, B. Tailoring Active Sites of Iron-Nitrogen-Carbon Catalysts for Oxygen Reduction in Alkaline Environment: Effect of Nitrogen-Based Organic Precursor and Pyrolysis Atmosphere. *Electrochim. Acta* **2021**, *391*, 138899. [CrossRef]
52. Ficca, V.C.A.; Santoro, C.; Marsili, E.; da Silva Freitas, W.; Serov, A.; Atanassov, P.; Mecheri, B. Sensing Nitrite by Iron-Nitrogen-Carbon Oxygen Reduction Electrocatalyst. *Electrochim. Acta* **2022**, *402*, 139514. [CrossRef]
53. Hess, F. Corrosion Mechanism and Stabilization Strategies for RuO_2 and IrO_2 Catalysts in the Electrochemical Oxygen Evolution Reaction. *Curr. Opin. Electrochem.* **2023**, *41*, 101349. [CrossRef]
54. Briguglio, N.; Siracusano, S.; Bonura, G.; Sebastián, D.; Aricò, A.S. Flammability Reduction in a Pressurised Water Electrolyser Based on a Thin Polymer Electrolyte Membrane through a Pt-Alloy Catalytic Approach. *Appl. Catal. B* **2019**, *246*, 254–265. [CrossRef]
55. Li, Y.; Li, Y.; Ding, Y.; Ma, J.; Das, P.; Zhang, B.; Wu, Z.-S.; Bao, X. Spatially Confined Sub-Nanometer Pt in RuO_2 Nanosheet as Robust Bifunctional Oxygen Electrocatalyst for Stabilizing Li-O_2 Batteries. *Chem Catal.* **2023**, 100658. [CrossRef]
56. He, X.; Tian, Y.; Huang, Z.; Xu, L.; Wu, J.; Qian, J.; Zhang, J.; Li, H. Engineering the Electronic States of Ni3FeN via Zinc Ion Regulation for Promoting Oxygen Electrocatalysis in Rechargeable Zn–air Batteries. *J. Mater. Chem. A* **2021**, *9*, 2301–2307. [CrossRef]
57. Vincent, I.; Lee, E.-C.; Kim, H.-M. Highly Cost-Effective Platinum-Free Anion Exchange Membrane Electrolysis for Large Scale Energy Storage and Hydrogen Production. *RSC Adv.* **2020**, *10*, 37429–37438. [CrossRef] [PubMed]
58. Vincent, I.; Lee, E.-C.; Kim, H.-M. Highly Active Ni–Fe Based Oxide Oxygen Evolution Reaction Electrocatalysts for Alkaline Anion Exchange Membrane Electrolyser. *Catalysts* **2022**, *12*, 476. [CrossRef]
59. Hu, B.; Yang, Y.; Cao, W.; Wang, X.; Zhou, C.; Mao, Y.; Ge, L.; Ran, R.; Zhou, W. Patchy Fe-N-C Supported Low-Loading Pt Nanoparticles as a Highly Active Cathode for Proton Exchange Membrane Fuel Cells. *J. Alloys Compd.* **2023**, *951*, 169867. [CrossRef]
60. Liu, X.; Tian, J.; Zhou, C.; Jiang, J.; Cheng, X.; Yang, L.; Wu, Q.; Wang, X.; Hu, Z. Constructing Membrane Electrodes of Low Pt Areal Loading with the New Support of N-Doped Carbon Nanocages for PEMFC. *FlatChem* **2023**, *40*, 100515. [CrossRef]
61. da Silva Freitas, W.; Mecheri, B.; Lo Vecchio, C.; Gatto, I.; Baglio, V.; Ficca, V.C.A.; Patra, A.; Placidi, E.; D'Epifanio, A. Metal-Organic-Framework-Derived Electrocatalysts for Alkaline Polymer Electrolyte Fuel Cells. *J. Power Sources* **2022**, *550*, 232135. [CrossRef]
62. da Silva Freitas, W.; Machado Pico, P.P.; D'Epifanio, A.; Mecheri, B. Nanostructured Fe-N-C as Bifunctional Catalysts for Oxygen Reduction and Hydrogen Evolution. *Catalysts* **2021**, *11*, 1525. [CrossRef]
63. Costa de Oliveira, M.A.; Mecheri, B.; D'Epifanio, A.; Zurlo, F.; Licoccia, S. Optimization of PGM-Free Cathodes for Oxygen Reduction in Microbial Fuel Cells. *Electrochim. Acta* **2020**, *334*, 135650. [CrossRef]
64. Andersen, S.M.; Dhiman, R.; Larsen, M.J.; Skou, E. Importance of Electrode Hot-Pressing Conditions for the Catalyst Performance of Proton Exchange Membrane Fuel Cells. *Appl. Catal. B* **2015**, *172–173*, 82–90. [CrossRef]
65. Yamada, M.; Watanabe, T.; Gunji, T.; Wu, J.; Matsumoto, F. Review of the Design of Current Collectors for Improving the Battery Performance in Lithium-Ion and Post-Lithium-Ion Batteries. *Electrochem* **2020**, *1*, 124–159. [CrossRef]
66. Zhu, P.; Gastol, D.; Marshall, J.; Sommerville, R.; Goodship, V.; Kendrick, E. A Review of Current Collectors for Lithium-Ion Batteries. *J. Power Sources* **2020**, *485*, 229321. [CrossRef]
67. Aguiló-Aguayo, N.; Espiñeira, P.P.; Manian, A.P.; Bechtold, T. Three-Dimensional Embroidered Current Collectors for Ultra-Thick Electrodes in Batteries. *RSC Adv.* **2016**, *6*, 69685–69690. [CrossRef]
68. Wang, H.; Yu, D.Y.W. Stainless Steel as Low-Cost High-Voltage Cathode via Stripping/Deposition in Metal-Lithium Battery. *Electrochim. Acta* **2019**, *298*, 186–193. [CrossRef]
69. Zhang, X.; Chu, Y.; Xiong, X.; Fan, Q.; Han, D.; Wu, C. CoP-Loaded BiVO4 for Highly Active and Robust Photocathodic Protection of 304 Stainless Steel. Mater. *Today Commun.* **2023**, *35*, 105848. [CrossRef]
70. Wang, J.-Y.; Kadier, A.; Hao, B.; Li, H.; Ma, P.-C. Performance Optimization of a Batch Scale Electrocoagulation Process Using Stainless Steel Mesh (304) Cathode for the Separation of Oil-in-Water Emulsion. *Chem. Eng. Process.-Process Intensif.* **2022**, *174*, 108901. [CrossRef]

71. Zhang, Y.; Merrill, M.D.; Logan, B.E. The Use and Optimization of Stainless Steel Mesh Cathodes in Microbial Electrolysis Cells. *Int. J. Hydrog. Energy* **2010**, *35*, 12020–12028. [CrossRef]
72. Daio, T.; Staykov, A.; Guo, L.; Liu, J.; Tanaka, M.; Matthew Lyth, S.; Sasaki, K. Lattice Strain Mapping of Platinum Nanoparticles on Carbon and SnO_2 Supports. *Sci. Rep.* **2015**, *5*, 13126. [CrossRef]
73. Mauger, S.A.; Pfeilsticker, J.R.; Wang, M.; Medina, S.; Yang-Neyerlin, A.C.; Neyerlin, K.C.; Stetson, C.; Pylypenko, S.; Ulsh, M. Fabrication of High-Performance Gas-Diffusion-Electrode Based Membrane-Electrode Assemblies. *J. Power Sources* **2020**, *450*, 227581. [CrossRef]
74. Sumboja, A.; Ge, X.; Zheng, G.; Goh, F.W.T.; Hor, T.S.A.; Zong, Y.; Liu, Z. Durable Rechargeable Zinc-Air Batteries with Neutral Electrolyte and Manganese Oxide Catalyst. *J. Power Sources* **2016**, *332*, 330–336. [CrossRef]
75. Wu, K.; Zhang, L.; Yuan, Y.; Zhong, L.; Chen, Z.; Chi, X.; Lu, H.; Chen, Z.; Zou, R.; Li, T.; et al. An Iron-Decorated Carbon Aerogel for Rechargeable Flow and Flexible Zn–air Batteries. *Adv. Mater.* **2020**, *32*, 2002292. [CrossRef]
76. Shao, Q.; Liu, J.; Wu, Q.; Li, Q.; Wang, H.; Duan, Q. In Situ Coupling Strategy for Anchoring Monodisperse Co9S8 Nanoparticles on S and N Dual-Doped Graphene as a Bifunctional Electrocatalyst for Rechargeable Zn–air Battery. *Nano-Micro Lett.* **2019**, *11*, 4. [CrossRef]
77. Shahbazi Farahani, F.; Rahmanifar, M.S.; Noori, A.; El-Kady, M.F.; Hassani, N.; Neek-Amal, M.; Kaner, R.B.; Mousavi, M.F. Trilayer Metal-Organic Frameworks as Multifunctional Electrocatalysts for Energy Conversion and Storage Applications. *J. Am. Chem. Soc.* **2022**, *144*, 3411–3428. [CrossRef]
78. Han, J.; Meng, X.; Lu, L.; Bian, J.; Li, Z.; Sun, C. Single-Atom Fe-Nx-C as an Efficient Electrocatalyst for Zinc-Air Batteries. *Adv. Funct. Mater.* **2019**, *29*, 1808872. [CrossRef]
79. Zhang, J.; Zhang, M.; Zeng, Y.; Chen, J.; Qiu, L.; Zhou, H.; Sun, C.; Yu, Y.; Zhu, C.; Zhu, Z. Single Fe Atom on Hierarchically Porous S, N-Codoped Nanocarbon Derived from Porphyra Enable Boosted Oxygen Catalysis for Rechargeable Zn–air Batteries. *Small* **2019**, *15*, 1900307. [CrossRef]
80. Niu, H.-J.; Wang, A.-J.; Zhang, L.; Feng, J.-J. Bioinspired One-Step Pyrolysis Fabrication of 3D Porous Co, N, P-Doped Carbon Nanosheets with Enriched CoNx Active Sites as High-Performance Bifunctional Oxygen Electrocatalyst for Rechargeable Zn–air Battery. *ACS Appl. Energy Mater.* **2020**, *3*, 2781–2790. [CrossRef]